

## Exploring the Thermodynamics of a Two-Dimensional Bose Gas

Tarik Yefsah, Rémi Desbuquois, Lauriane Chomaz, Kenneth J. Günter, and Jean Dalibard

*Laboratoire Kastler Brossel, CNRS, UPMC, Ecole Normale Supérieure, 24 rue Lhomond, F-75005 Paris, France*

(Received 30 May 2011; revised manuscript received 11 July 2011; published 19 September 2011)

Using *in situ* measurements on a quasi-two-dimensional, harmonically trapped  $^{87}\text{Rb}$  gas, we infer various equations of state for the equivalent homogeneous fluid. From the dependence of the total atom number and the central density of our clouds with chemical potential and temperature, we obtain the equations of state for the pressure and the phase-space density. Then, using the approximate scale invariance of this 2D system, we determine the entropy per particle and find very low values (below  $0.1k_B$ ) in the strongly degenerate regime. This shows that this gas can constitute an efficient coolant for other quantum fluids. We also explain how to disentangle the various contributions (kinetic, potential, interaction) to the energy of the trapped gas using a time-of-flight method, from which we infer the reduction of density fluctuations in a nonfully coherent cloud.

DOI: 10.1103/PhysRevLett.107.130401

PACS numbers: 03.75.-b, 05.10.Ln, 42.25.Dd

The physical properties of homogeneous matter at thermal equilibrium are characterized by an equation of state (EOS), i.e., a relationship between some relevant state variables. For a fluid of particles, possible EOS's consist of expressions of pressure, density, or entropy as functions of temperature  $T$  and chemical potential  $\mu$ . In the ideal case the EOS is known in any dimension for a Bose or Fermi gas. In the presence of interactions, one has to resort to approximations or numerical calculations, and a comparison with experiments is crucial to test their validity. Trapped atomic gases at thermal equilibrium provide a powerful tool for this purpose [1]. Within the local density approximation (LDA), intensive state variables take at a point  $\mathbf{r}$  in the trap the same value as in a homogenous system with the same temperature and the shifted chemical potential  $\mu - V(\mathbf{r})$ , where  $V(\mathbf{r})$  is the confining potential.

The case of an interacting two-dimensional Bose fluid is particularly interesting in this context. Firstly, at non-zero temperature the Mermin-Wagner theorem precludes Bose-Einstein condensation [2,3]. Therefore the EOS is expected to be continuous at any point, in spite of the existence of a superfluid, infinite-order phase transition, which is of the Berezinskii-Kosterlitz-Thouless (BKT) type [4,5]. Secondly, the EOS exhibits an approximate scale invariance [6] in the regime of relatively weak atomic interactions which is of interest here. It originates from the fact that the interaction strength is an energy-independent dimensionless coefficient  $\tilde{g}$  ( $\ll 1$ ), and thus provides no energy, nor length scale, in contrast with the 1D or 3D cases. This implies, in particular, that dimensionless thermodynamic variables such as the phase-space density  $\mathcal{D}$  or the entropy per particle  $\mathcal{S}$  are functions of the ratio  $\mu/k_B T$  only, with  $\tilde{g}$  as a parameter.

Recent experiments with trapped 2D Bose gases have demonstrated the existence of a BKT-type transition. One line of investigation exploited matter-wave interference to monitor the appearance of an extended coherence in the

sample [7,8], and another approach used a time-of-flight (TOF) technique to measure the momentum distribution of the gas [9]. The scale invariance for  $\mathcal{D}$  was verified in [10]. In this Letter we present a detailed experimental investigation of several thermodynamic properties of a 2D Bose gas. We describe measurements of the EOS for the pressure from a count of the total number of trapped atoms, for a wide range of thermodynamic parameters. From the same set of data we use the central spatial density to access the EOS for phase-space density. Combining these two EOS's with the scale invariance we obtain the EOS for the entropy per particle. We show that this quantity rapidly decreases around the superfluid transition and then approaches zero in the highly degenerate regime. We also present an original method to extract from a TOF the various contributions (kinetic, potential, interaction) to the total energy of the trapped gas. This method is applicable to any low-dimensional fluid. Here it shows that density fluctuations of our 2D Bose gas are essentially suppressed even when its thermal, noncoherent fraction is significant.

Our 2D Bose gases are prepared along the lines detailed in [11]. We start with a 3D Bose-Einstein condensate of  $^{87}\text{Rb}$  atoms confined in a magnetic trap in their  $F = m_F = 2$  internal ground state with an adjustable temperature. We slice a horizontal sheet of atoms with an off-resonant, blue-detuned laser beam with an intensity node in the plane  $z = 0$ . It provides a strong confinement along the  $z$  axis with oscillation frequency  $\omega_z/2\pi = 2.0(2)$  kHz. The interaction strength is  $\tilde{g} = \sqrt{8\pi}a/\ell_z = 0.109(5)$ , where  $a$  is the 3D scattering length and  $\ell_z = \sqrt{\hbar/m\omega_z}$ . The energy  $\hbar\omega_z$  is similar to or larger than the thermal energy  $k_B T$  and the interaction energy per particle. Our gas is thus in the so-called quasi-2D regime [12], where most of the atoms occupy the ground state of the vibrational motion along  $z$ , making it thermodynamically 2D, but where collisions still keep their 3D character since  $a = 5.3$  nm  $\ll \ell_z = 240$  nm. The magnetic trap provides

a quasi-isotropic confinement in the  $xy$  plane with frequency  $\omega/2\pi = 20.6(1)$  Hz [13].

After an equilibration time of 3 s in the combined magnetic-laser trap, we measure the *in situ* density distribution of the gas by performing absorption imaging with a probe beam propagating along  $z$ . The conventional procedure where one uses a weak probe beam with an intensity  $I$  well below the saturation intensity  $I_{\text{sat}}$  is problematic in this context [11]. Indeed, for the relevant range of temperatures (40–150 nK), the atomic thermal wavelength  $\lambda_T = (2\pi\hbar^2/mk_B T)^{1/2}$  is comparable to the optical wavelength used for probing,  $\lambda_{\text{opt}} = 780$  nm. Consequently, in the highly degenerate region of the gas ( $\mathcal{D} \equiv n\lambda_T^2 \gg 1$ ), the average distance between neighboring atoms  $n^{-1/2}$  is much smaller than  $\lambda_{\text{opt}}$  and the absorption of a weak probe is strongly perturbed by collective effects. To circumvent this problem we probe the gas with a short pulse (duration  $\sim 2 \mu\text{s}$ ) of an intense probe beam (typically  $I/I_{\text{sat}} = 40$ –100) [14]. The interaction of any given atom with light is then nearly independent of its neighbors.

High-intensity imaging, which was also used in [10], provides a faithful measurement of the atomic distribution in the central region of the trap, where the density is large. However, the quality of the images suffers from a large photon shot noise, which spoils the detection of the low-density regions of the cloud [Fig. 1(a)]. In order to reliably probe these regions on which we base our determination of  $T$  and  $\mu$ , we complement the high-intensity imaging procedure by the conventional low-intensity one [Fig. 1(b)]. In practice, for each set of parameters we perform one run of the experiment with high-intensity imaging and one with low-intensity imaging immediately after. The reproducibility is checked by acquiring several pairs of images for a given set of experimental parameters.

The procedure for image processing is detailed in the Supplemental Material [15]. In short, for each pair of images it provides the temperature  $T$ , the chemical potential at center  $\mu$ , and the density  $n(\mathbf{r})$  at any pixel of the image. We assume that the atoms in the excited states of the  $z$  motion are well described by the Hartree-Fock mean-field (HFMF) theory [9,16–18]. We thus self-consistently calculate the populations of these states and subtract them from  $n(\mathbf{r})$  in order to obtain the density distribution  $n_0(\mathbf{r})$  in the ground state. The validity of this procedure was checked by analyzing the results of a quantum Monte Carlo calculation for parameters similar to ours [19].

We start our thermodynamic analysis by inferring the pressure  $P(\mu, T)$  of the homogeneous gas from our measurements. Here we adapt to the 2D case the technique presented in [1], which has been used successfully in 3D for Fermi gases [20]. We show that  $P(\mu, T)$  is directly related to the atom number  $N_0 = \int n_0(\mathbf{r}) d^2r$  in our harmonic trap. Indeed, the LDA relates  $n_0(\mathbf{r})$  to the density of the homogeneous gas  $n_{\text{hom}}^{(2D)}[\mu - V(\mathbf{r}), T]$  [21]. For an

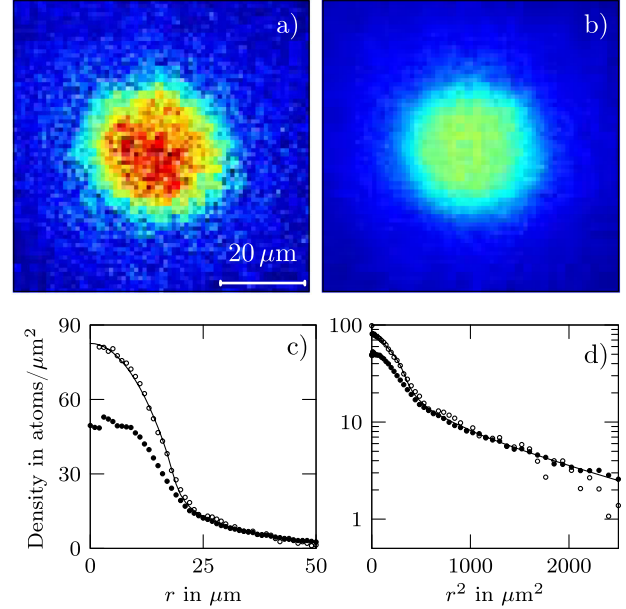


FIG. 1 (color online). Absorption imaging of quasi-2D clouds of  $^{87}\text{Rb}$  atoms. (a) Image obtained with a short pulse ( $\sim 2 \mu\text{s}$ ) of an intense probe beam ( $I/I_{\text{sat}} = 40$ ). (b) Image obtained with a longer pulse ( $50 \mu\text{s}$ ) of a weak probe beam ( $I/I_{\text{sat}} = 0.5$ ). The processing of images (a) and (b) is detailed in the Supplemental Material [15]. (c),(d) Radial density profiles for image (a) (○) and image (b) (●) in linear (c) and logarithmic (d) scales. The solid line is the prediction for the total density ( $T = 133$  nK,  $\mu/k_B = 47$  nK). It includes the populations of the excited states of the  $z$  motion calculated using HFMF theory, and the population of the ground state calculated from (i) the prediction of [6] in the range where it is available [ $\alpha \equiv \mu/k_B T \in (-0.2, 0.6)$ ], (ii) the HFMF theory for  $\alpha < -0.2$ , and (iii) the Thomas-Fermi approximation  $\mu = \hbar^2 \tilde{g} n/m$  for  $\alpha > 0.6$ .

isotropic harmonic potential  $V(\mathbf{r}) = m\omega^2 r^2/2$  the total atom number is

$$N_0 = \frac{2\pi}{m\omega^2} \int_{-\infty}^{\mu} n_{\text{hom}}^{(2D)}(\mu', T) d\mu', \quad (1)$$

and using the thermodynamic relation  $n_{\text{hom}}^{(2D)} = (\partial P/\partial \mu)_T$ , we find  $N_0 = (2\pi/m\omega^2)P(\mu, T)$ . Introducing the dimensionless quantity  $\mathcal{P} = P\lambda_T^2/k_B T$ , which we refer to as the reduced pressure, we then obtain

$$\mathcal{P}(\mu, T) = \left(\frac{\hbar\omega}{k_B T}\right)^2 N_0, \quad (2)$$

where  $\omega$  is to be replaced by the geometrical mean of  $\omega_x$  and  $\omega_y$  for a nonisotropic potential. Our results are summarized in Fig. 2(a), where we plot  $\mathcal{P}$  deduced from Eq. (2) as a function of  $\mu/k_B T$ . The temperatures of the data entering in this plot range from 40 to 150 nK. The fact that all data points collapse on the same line shows that  $\mathcal{P}$  is a function of the ratio  $\mu/k_B T$  only, as expected from the scale invariance of the system. The HFMF theory is represented by a continuous line in the normal region and by a

dotted line in the superfluid region. The dashed line is the Thomas-Fermi prediction at zero temperature  $\mathcal{P} = \pi(\mu/k_B T)^2/\tilde{g}$ . The gray area is the parameter subspace accessible to an ideal Bose gas. Interestingly, although the phase-space density  $\mathcal{D}$  can take arbitrarily large values, one can show in the ideal gas case that the reduced pressure  $\mathcal{P} = \text{Li}_2(z) \leq \pi^2/6$ , where  $\text{Li}_2$  is the dilogarithm function and  $z = \exp(\mu/k_B T)$  ( $z \leq 1$  for an ideal Bose gas).

In Fig. 2(b) we show our measurements for the phase-space density  $\mathcal{D}$ , obtained from the central density of each cloud. In the wide gray line we plot the prediction of [6], which is in good agreement with our results. A further confirmation of this agreement is shown in Fig. 1(c), where we plot in the solid line the numerically generated profile using [6] for the fitted  $T$  and  $\mu$ . A measurement of  $\mathcal{D}(\mu/k_B T, \tilde{g})$  was also reported in [10] for a quasi-2D cesium gas, for  $\tilde{g}$  ranging from 0.05 to 0.26. Our results agree well with those measurements over the covered range ( $\mathcal{D} < 20$  in [10] for  $\tilde{g}$  similar to ours).

From our measurements of  $\mathcal{P}$  and  $\mathcal{D}$  we also obtain the equation of state for the entropy per particle  $\mathcal{S}(\mu, T)$ :

$$\frac{\mathcal{S}}{k_B} = 2 \frac{\mathcal{P}}{\mathcal{D}} - \frac{\mu}{k_B T}, \quad (3)$$

which can be derived starting from the entropy per unit area  $s = (\partial P/\partial T)_\mu$ , assuming the EOS for  $\mathcal{P}$  to be scale invariant [22]. The corresponding result is shown in Fig. 2(c). As expected,  $\mathcal{S}$  is large in the nondegenerate regime and rapidly decreases around  $\mu/k_B T \approx 0.17$ , where the superfluid transition is expected for our value of  $\tilde{g}$  [23]. Above this point our results are located between the HFMF prediction, which provides an upper bound since it overestimates density fluctuations, and the strictly

zero value for the Thomas-Fermi regime. The average value of the entropy per particle for our data points with large phase-space density ( $\mu/k_B T > 0.5$ ) is  $\mathcal{S} = 0.06(1)k_B$  only. For comparison the entropy per particle reported in [24] for a 2D Mott insulator is  $\sim 0.3k_B$ . Note that since the BKT transition is of infinite order, one does not expect any discontinuous change for  $\mathcal{P}$ ,  $\mathcal{D}$ , or  $\mathcal{S}$  at the superfluid transition for an infinite homogeneous fluid, although the superfluid density jumps suddenly from 0 to  $4/\lambda_T^2$  [25].

We now turn to the last part of our study, where we illustrate how to measure the various contributions to the energy of our trapped 2D gases: potential energy  $E_p$  in the external trapping potential, kinetic energy of the particles  $E_k$ , and interaction energy between atoms  $E_i$ . We first point out the simple relation  $E_p = E_k + E_i$ , obtained from the virial theorem assuming 2D contact interaction. We measure  $E_p = \int n_0(\mathbf{r})V(\mathbf{r})d^2r$  from an *in situ* image, but we still need to disentangle the contributions of  $E_k$  and  $E_i$  to the total energy. This can be done by abruptly switching off interactions at time  $t = 0$ , either via a Feshbach resonance or effectively by using a ‘‘one dimensional’’ TOF described below. Each particle then undergoes a free harmonic motion  $\mathbf{r}(t) = \cos(\omega t)\mathbf{r}(0) + \sin(\omega t)\mathbf{v}(0)/\omega$ . The potential energy after a time  $t$  following the switching off of the interactions is

$$E_p(t) = E_p(0)\cos^2(\omega t) + E_k(0)\sin^2(\omega t), \quad (4)$$

where we used the fact that the correlation  $\langle \mathbf{r}(0) \cdot \mathbf{v}(0) \rangle$  is zero at thermal equilibrium. Thus we can extract  $E_k(0)$  from the time evolution of  $E_p$ , which we obtain from the density profiles at different times  $t$ .

In order to implement this procedure, we perform the 1D TOF mentioned above by abruptly switching off the laser

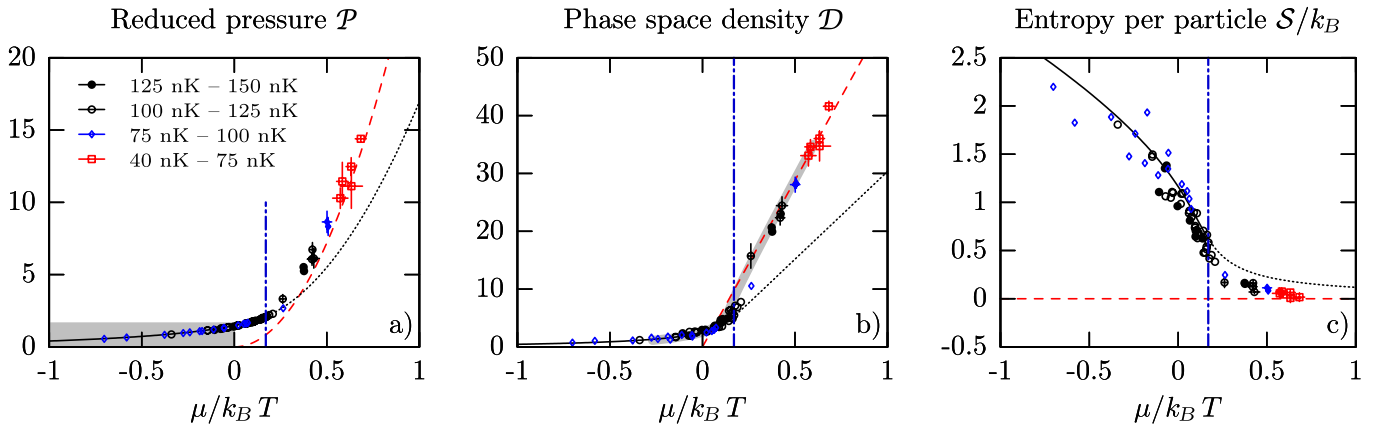


FIG. 2 (color online). Equations of state for (a) the reduced pressure  $\mathcal{P}$ , (b) the phase-space density  $\mathcal{D}$ , and (c) the entropy per particle  $\mathcal{S}$ . The HFMF prediction is plotted in black full line and extended in dotted line beyond the expected superfluid transition. The dashed (red) line is the Thomas-Fermi prediction. In (a) the gray shaded area indicates the region of parameter space accessible to an ideal gas. In (b) the thick gray line indicates the prediction from [6]. For  $\mu/k_B T > 0.2$ , data obtained for the same control parameters (trap loading time and evaporative cooling ramp) have been grouped and error bars indicate standard deviation of the measurement. For  $\mu/k_B T < 0.2$ , data are displayed for individual images, thus with no error bars. The vertical dash-dotted line (blue) indicates the prediction [23] for the superfluid transition.

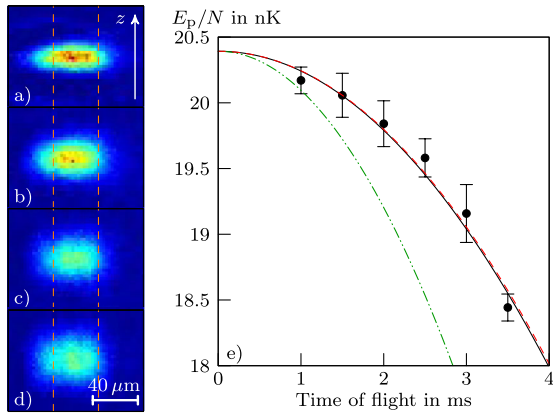


FIG. 3 (color online). (a)–(d) Side view of a cloud initially in the 2D regime and expanding along  $z$  once the laser providing the confinement in this direction has been switched off. (a)  $t = 1$  ms, (b)  $t = 2$  ms, (c)  $t = 3$  ms, and (d)  $t = 4$  ms. (e) Time evolution of the potential energy  $E_p$ . The different lines represent a fit to the data of a parabola (solid black line), the time evolution assuming flattened density fluctuations (dashed red line) and the one expected for a dilute noncondensed gas (dash-dotted green line).

providing the confinement along  $z$  while keeping the magnetic confinement in the  $xy$  plane. The gas then expands very fast along the initially strongly confined direction  $z$ , as shown in Figs. 3(a)–3(d), and interactions between particles drop to a negligible value after a time of a few  $\omega_z^{-1}$ , where  $\omega_z^{-1} \sim 100 \mu\text{s}$ . The subsequent evolution in the  $xy$  plane occurs on a longer time scale given by  $\omega^{-1} \sim 8$  ms. From Eq. (4) and  $E_k(0) < E_p(0)$ , we expect the size of the gas to decrease for  $t \lesssim \omega^{-1}$ , which can be understood in simple physical terms. The equilibrium state of the 2D gas results from a balance between the trapping potential, which tends to compress the gas, and the kinetic and interaction energies, which tend to increase its area. When interaction energy drops to zero, the equilibrium is broken and the gas implodes in the  $xy$  plane. A similar 1D TOF technique was used recently by Cornell and co-workers (Boulder) with the value of  $t$  fixed at  $\pi/2\omega$  [9]. At this time the initial momentum distribution is converted into position distribution and can thus be measured accurately [26].

In Fig. 3 we show an example of measurement of  $E_p(t)$  for a gas with  $N_0 = 6.1 \times 10^4$ ,  $T = 72$  nK, and  $\mu/k_B T = 0.59$ . From the contraction of the gas, we infer  $E_k/E_p = 0.56(3)$ , from which we deduce  $E_i/E_p = 0.44(3)$  using the virial theorem. This configuration is thus neither completely in the very dilute regime ( $E_i \ll E_k \sim E_p$ ) nor in the Thomas-Fermi regime ( $E_k \ll E_i \sim E_p$ ) and contains comparable thermal and quasicohherent fractions.

The measurement of  $E_i$  is of particular interest in this case since it gives access to the density fluctuations in the gas. Indeed, by definition  $E_i = (\hbar^2 \tilde{g}/2m) \int \langle n_0^2(\mathbf{r}) \rangle d^2r = (\hbar^2 \tilde{g}/2m) \mathcal{F} \int \langle n_0(\mathbf{r}) \rangle^2 d^2r$  [27], where we have introduced

the parameter  $\mathcal{F}$  that characterizes the degree to which the density fluctuations are reduced. In the limiting case of a dilute, noncondensed gas, one expects  $\mathcal{F} = 2$ , since  $\langle n_0^2 \rangle = 2\langle n_0 \rangle^2$ , while in the opposite limit of a “flattened” density profile  $\mathcal{F} = 1$ . Since our measurement provides us with  $E_i$ , we can infer the value of  $\mathcal{F}$ , from comparison with the quantity  $(\hbar^2 \tilde{g}/2m) \int \langle n_0(\mathbf{r}) \rangle^2 d^2r$ , calculated using the *in situ* density profile  $n_0$ . For the conditions of Fig. 3(e), we find  $\mathcal{F} = 1.1(1)$ , very close to the value 1 for flattened density fluctuations. Note that this is obtained for a gas still far from the Thomas-Fermi limit since  $E_k \sim E_i$ . This “early” reduction of density fluctuations is an important ingredient for the proper operation of the BKT mechanism. This presuperfluid phase, whose existence was also inferred by different methods in [8–10], constitutes a medium that can support vortices, which pair at the superfluid threshold.

In conclusion we presented in this Letter various aspects of the thermodynamics of a 2D Bose gas, investigating first the EOS’s for the pressure, the phase-space density, and the entropy and confirming their scale invariance. We point out that the entropy per particle drops notably below  $0.1k_B$  beyond the transition point. With such a low entropy a 2D Bose gas can constitute excellent coolants for other quantum fluids such as 2D Fermi gases [28]. We also presented a method that allows one to extract the various contributions to the total energy of the system. By applying it to a degenerate but not fully coherent 2D cloud, we find that density fluctuations are nearly frozen, marking the presuperfluid phase.

We thank Gordon Baym, Yvan Castin, Markus Holzmann, Werner Krauth, Christophe Salomon, Sandro Stringari, and Martin Zwierlein for helpful discussions. We are grateful to Benno Rem for his help at an early stage of this project. We are indebted to Aviv Keshet for letting us use the computer code that he wrote for experimental control. This work is supported by IFRAF and ANR (project BOFL).

- 
- [1] T.-L. Ho and Q. Zhou, *Nature Phys.* **6**, 131 (2009).
  - [2] N.D. Mermin and H. Wagner, *Phys. Rev. Lett.* **17**, 1133 (1966).
  - [3] P.C. Hohenberg, *Phys. Rev.* **158**, 383 (1967).
  - [4] V.L. Berezinskii, *Sov. Phys. JETP* **34**, 610 (1971).
  - [5] J.M. Kosterlitz and D.J. Thouless, *J. Phys. C* **6**, 1181 (1973).
  - [6] N.V. Prokof’ev and B.V. Svistunov, *Phys. Rev. A* **66**, 043608 (2002).
  - [7] Z. Hadzibabic *et al.*, *Nature (London)* **441**, 1118 (2006).
  - [8] P. Cladé *et al.*, *Phys. Rev. Lett.* **102**, 170401 (2009).
  - [9] S. Tung *et al.*, *Phys. Rev. Lett.* **105**, 230408 (2010).
  - [10] C.-L. Hung *et al.*, *Nature (London)* **470**, 236 (2011).
  - [11] S.P. Rath *et al.*, *Phys. Rev. A* **82**, 013609 (2010).
  - [12] D.S. Petrov, M. Holzmann, and G.V. Shlyapnikov, *Phys. Rev. Lett.* **84**, 2551 (2000).

- [13] The residual anisotropy of the trap is  $|\omega_x - \omega_y|/\omega < 6\%$  where  $\omega = (\omega_x \omega_y)^{1/2}$ ; it plays no significant role in the subsequent analyses. Our procedure to handle slight deviations with respect to harmonicity is described in the Supplemental Material [15].
- [14] G. Reinaudi *et al.*, *Opt. Lett.* **32**, 3143 (2007).
- [15] See Supplemental Material at <http://link.aps.org/supplemental/10.1103/PhysRevLett.107.130401> for a detailed description of the imaging technique and production and analysis of the density profiles.
- [16] Z. Hadzibabic *et al.*, *New J. Phys.* **10**, 045006 (2008).
- [17] R. N. Bisset, D. Baillie, and P. B. Blakie, *Phys. Rev. A* **79**, 013602 (2009).
- [18] M. Holzmann, M. Chevallier, and W. Krauth, *Phys. Rev. A* **81**, 043622 (2010).
- [19] M. Holzmann and W. Krauth, *Phys. Rev. Lett.* **100**, 190402 (2008).
- [20] S. Nascimbène *et al.*, *Nature (London)* **463**, 1057 (2010).
- [21] The LDA holds for short-range interactions when the spatial density is nearly constant over the microscopic length scales set by  $\lambda_T$  and by the healing length  $\xi = (\tilde{g}n)^{-1/2}$ .
- [22] A similar method has been used for a 3D Fermi gas at unitarity, Martin Zwierlein (private communication).
- [23] N. V. Prokof'ev, O. Ruebenacker, and B. V. Svistunov, *Phys. Rev. Lett.* **87**, 270402 (2001).
- [24] J. F. Sherson *et al.*, *Nature (London)* **467**, 68 (2010).
- [25] D. R. Nelson and J. M. Kosterlitz, *Phys. Rev. Lett.* **39**, 1201 (1977).
- [26] I. Shvarchuck *et al.*, *Phys. Rev. Lett.* **89**, 270404 (2002).
- [27]  $\langle n_0(\mathbf{r})n_0(\mathbf{r}') \rangle$  here stands for  $\langle \hat{\psi}^\dagger(\mathbf{r})\hat{\psi}^\dagger(\mathbf{r}')\hat{\psi}(\mathbf{r}')\hat{\psi}(\mathbf{r}) \rangle$ , where  $\hat{\psi}^\dagger(\mathbf{r})$  creates a particle in  $\mathbf{r} = (x, y)$  and in the ground state of the  $z$  motion; see, e.g., W. Ketterle and H.-J. Miesner, *Phys. Rev. A* **56**, 3291 (1997).
- [28] B. Fröhlich *et al.*, *Phys. Rev. Lett.* **106**, 105301 (2011).